J. Fluid Mech. (1990), *vol.* 218, *pp.* 355–376
Printed in Great Britain

Transient bubbles interacting with an attached cavity and the boundary layer

By L. BRIANÇON-MARJOLLET†, J. P. FRANC AND J. M. MICHEL

Institut de Mécanique de Grenoble, B.P. 53 X, 38041 Grenoble Cedex, France

(Received 2 March 1989 and in revised form 21 November 1989)

Experiments on two-dimensional cavitating hydrofoils show important differences in global behaviour of flows according to the population of air nuclei conveyed by the liquid. By means of visualization techniques and flow modelling, the major features of attached-cavity flows and transient-bubble flows are revealed. The main topics of the paper are: cavitation inception in either regime, hydrofoil saturation and the sweeping away of a cavity by bubbles. The main conditions for the validity of the λ^{-3} similitude rule are delineated. Special attention is given to the mechanism of interaction between the exploding bubbles, the attached cavity and the boundary layer. Estimates of the critical number of active nuclei for saturation and cavity suppression which agree with experimental results are given.

1. Introduction

The present paper is designed to complete two previous studies (Franc & Michel 1985, 1988, hereinafter referred to as FM 1985 or FM 1988) in which the link between the detachment of a developed cavity and the laminar separation of the boundary layer was particularly demonstrated, both in a steady and an unsteady flow. That link, emphasized before by several authors for incipient cavitation (e.g. Arakeri & Acosta 1973; Van der Meulen 1980), operates fully when the liquid is strongly deaerated and thus able to sustain negative pressures. The situation is different if the liquid contains gas nuclei, or microbubbles, which can initiate the rupture of the continuous medium in an easier way: the microbubbles, whose size stability primarily depends on the local pressures they experience, explode in places where cavitation would not otherwise occur. The paper also focuses on the influence of the gas nuclei concentration; which involves the description of cavitation regimes with transient exploding bubbles, their comparison with the attached-cavitation regimes and the analysis of the conditions which allow either regime to appear and to spread out in the low-pressure region of a liquid flow.

It has been believed for a long time that the influence of viscosity together with that of the nuclei are responsible for most scale effects in cavitation (Holl & Wislicenus 1961; Knapp, Daily & Hammitt 1970), i.e. the discrepancies between the behaviour of actual cavitating flows and the predictions of theoretical models which are restricted to non-viscous liquids, unable to sustain pressures lower than the vapour pressure. Such effects are revealed, for instance, by the differences in cavitation patterns, and thence in force coefficients, which are produced on identical

† Present address: Grand Tunnel Hydrodynamique, Bassin d'Essais des Carènes 27100, Val de Reuil, France.

bodies when tested in different cavitation facilities under similar overall hydrodynamic conditions (Lindgren & Johnsson 1966). However, despite its importance when drawing up similarity rules in naval architecture and turbomachinery, a detailed study of the influence of the nuclei has been delayed owing to the technical difficulties of controlling the nuclei population (Lecoffre 1987). Indeed, it was only in 1975 that Albrecht & Bjorheden presented the first description of a generator of nuclei, producing small bubbles of about 0.2 mm in diameter, together with experimental results demonstrating the importance of the effect of the nuclei on the threshold of incipient cavitation and the value of the global force coefficients. Later, Henry, Lecoffre & Larroze (1980) drew attention to the following similarity law which had previously been mentioned by Holl & Wislicenus (1961): given a prototype flow and a geometrically similar model, cavitating flows with transient bubbles cannot be geometrically similar unless the ratio of active nuclei concentrations is about $1/\lambda^3$. That rule simply means that the numbers of active nuclei in homologous liquid volumes must be equal. Although not theoretically sufficient, when considering the explosion conditions of each nucleus, some global results on the thrust and lift coefficients presented by Henry *et al.* and later by Le Goff & Lecoffre (1982) tend to support the rule's validity for industrial purposes. Finally, it should be mentioned that Avellan *et al.* (1986) introduced the concept of saturation of a cavitating flow in order to describe the limiting effect of high nuclei concentrations on the efficiency of turbine models.

Here we approach the problem of the influence of nuclei from a fundamental viewpoint by examining several different two-dimensional cavitating flows around a NACA 16209 hydrofoil, a shape that is known for giving a nearly uniform pressure distribution over its upper side at small incidences. First, flows of strongly deaerated water are considered for which, as shown in FM (1985), only attached cavities appear. In that reference case the main adjustable parameters are the Reynolds number, the cavitation number and the angle of attack which causes the longitudinal pressure gradient to vary. Also, the turbulence level, which is determined by the design of the hydrodynamic tunnel, has to be set among the inlet parameters as it contributes to the excitation of transition to turbulence inside the boundary layer and thus can prevent cavitation from being attached to the wall. Secondly, the hydrodynamic tunnel water quality is modified by the use of a nuclei control system, composed of a nuclei generator and a nuclei measurement device, installed upstream of the tunnel test section.

In both cases the domains of the various cavitating regimes are determined. As expected, they exhibit considerable differences which are connected to the different mechanisms involved in cavitation inception (Arakeri & Acosta 1976; Lecoffre & Bonnin 1979). The case of small values of both cavitation number and incidence deserves special attention: with deaerated water, a cavity is attached on the rear part of the foil behind the laminar separation of the boundary layer; then the hydrodynamic conditions allow the added nuclei to grow and become macroscopic bubbles. When the nuclei concentration is large enough, the bubbles sweep away the previous cavity and possibly form an almost continuous vapour medium on the downstream part of the hydrofoil, which is said to be saturated by transient bubbles. Such saturation can be modelled on the basis of simple assumptions, thus enabling an estimation of the required nuclei concentration. On the other hand, understanding the cavity sweeping needs a deeper insight into the interaction between the boundary layer and the exploding bubbles. In this respect, some remarks made by Gates & Acosta (1978) are particularly useful since those authors observed that laminar

separation on a hemispherical-nose body 'became unsteady and was diminished, if not eliminated', by the effect of an increasing number of nuclei.

By means of visualization techniques – dye injection, photography under short-time flash lighting and rapid films – several interaction effects between individual exploding bubbles and the boundary layer are illustrated and analysed. It appears that an exploding bubble influences the attached cavity via the turbulent spot that it can produce in the boundary layer. That mechanism is consistent with Gates & Acosta's conjectures and the conclusions of our previous investigations. It makes it possible to estimate the active nuclei concentration required for the suppression of a developed cavity. A consequence is that nuclei have no practical effect on most leading-edge cavities.

In §2 the physical background and the numerical models we are using are outlined, while § 3 contains the description of the experimental set-up and conditions. Sections 4 and 5 are devoted to the global results obtained respectively without and with the nuclei seeding. Special attention is then paid to the conditions of incipient cavitation and to saturation by transient bubbles. Finally, §6 studies the interaction between bubbles, the cavity and the boundary layer.

2. Flow modelling

Here we give a short account of the rather simple physical models that we use when analysing our experimental conditions and results, particularly in relation to the following points: the nuclei stability, the radial velocity of exploding bubbles and their motion in the hydrofoil vicinity. The last point is connected to the so-called screening effect, that is the possibility for a bubble to pass round the high-pressure region and thus to be deviated from the oncoming streamline. It will be noted that air diffusion is not taken into account in the present work, although, should the occasion arise, it might influence the growth of nuclei entrapped in the separated region downstream of the laminar boundary-layer separation (Parkin & Baker 1988). Such small bubbles, almost attached to the local reverse flow, were observed at the nose of hemispherical bodies by Arakeri & Acosta (1973) and they are believed to produce the so-called 'bubble-ring' cavitation pattern (Holl & Carroll 1979). However, that configuration does not appear in our experiments, possibly because of the low value of the dissolved air content in the water. Thus the mechanisms we retain are dynamical and not diffusive in nature.

Concerning the size stability of a small spherical bubble, it is generally accepted (Knapp *et al.* 1970) that the bubble remains stable as long as the external pressure is larger than a critical value p_c given by

$$p_v - p_c = \frac{4}{3}\frac{S}{R_c}, \tag{1}$$

in which S is the liquid surface tension, p_v is the vapour pressure at the flow temperature, and R_c is the critical radius. R_c depends on the initial size of the bubble under reference conditions, i.e. on the amount of gas inside the bubble. In that static model, three main assumptions are made: (i) the liquid medium is able to stay in a thermally metastable state under pressures lower than p_v; (ii) at the bubble interface, only the surface tension of the liquid plays a role, excluding the effects of impurities and surfactants; (iii) the gas transfer through the bubble interface is negligibly small. Then p_c or R_c suffices to characterize a particular bubble. In our experimental case, the measurements give critical pressures of between 1000 Pa and

-20000 Pa approximately; the corresponding critical radii are 75 μm and 4 μm respectively.

The dynamical study of any macroscopic bubbles conveyed by the liquid flow in a given pressure field is beyond our scope. However, the experimental results suggest an important simplification with respect to that general case: as seen from photographs and films, the shape of a number of bubbles growing near the hydrofoil is – except from several cases which will be examined later – not too far from a hemisphere, at least during the explosion phase. Thus, the symmetry defects due to the pressure gradient are not too important and the spherical symmetry makes the bubble modelling a classical matter; it is relatively easy to consider the behaviour of a bubble in a variable pressure field (Plesset & Prosperetti 1977) and a bubble which travels through the hydrofoil pressure field (Johnson & Hsieh 1966; Voinov 1973). In the first configuration, the governing equation is that of Rayleigh–Plesset:

$$R\ddot{R} + \tfrac{3}{2}\dot{R}^2 = \frac{p(R) - p_\infty(t)}{\rho} \tag{2}$$

in which ρ is the liquid density, $R(t)$ is the variable bubble radius, $p_\infty(t)$ the external pressure and $p(R)$ is equal to the sum of the vapour and gas partial pressure inside the bubble, minus the surface tension term $2S/R$ and the viscous term $4\mu\dot{R}/R$. If the bubble explodes under a constant underpressure $p_v - p_\infty$, the last terms become negligible after a short time and $\dot{R}$ tends to a constant value $\dot{R}_\ell$ given by

$$\dot{R}_\ell = \left(\frac{2}{3}\frac{p_v - p_\infty}{\rho}\right)^{\frac{1}{2}}. \tag{3}$$

In order to fit the Rayleigh–Plesset equation to the experimental case, $p_\infty(t)$ is identified with the local pressure near the hydrofoil. The calculation of the bubble trajectories is carried out either by assuming that the bubbles follow the liquid particles along the streamlines, or by using the Hsieh equation for the bubble free paths.

At this point, the pressure field around the non-cavitating or cavitating hydrofoil must be calculated. This is done by means of potential, nonlinear methods (Pellone & Rowe 1981; Lemonnier & Rowe 1988) which use discrete singularities on the foil surface, with the external boundaries of the experimental configuration – channel bottom and channel free surface – being accounted for by the image method. Figure 1 shows examples of calculated pressure distributions over a foil held at zero incidence. The pressure coefficient at M is defined by $C_p = 2(p_M - p_r)/\rho U^2$, where U is the free-stream velocity and p_r the reference pressure upstream of the foil. In the non-cavitating case, the pressure coefficient is nearly constant on the upper side and its minimum value is -0.302. In the supercavitating case, velocity continuity is assumed at the detachment abscissae and the cavity length is measured from the experiment. In other cases, the upper-side detachment point was determined, as in FM (1985), by combining potential-flow and boundary-layer computations, and using the criterion of proximity between laminar separation and cavity detachment. As soon as the basic boundary problem is solved, it is possible to calculate the velocity and the pressure at any point inside the flow field and map the isobaric curves in order to determine approximately the domain of nuclei activation. Examples of such mappings are given in figure 2. Comparison between (*a*) and (*c*) shows how much a cavity, even when attached to the downstream part of the foil, modifies the pressure field and reduces its activation capacity.

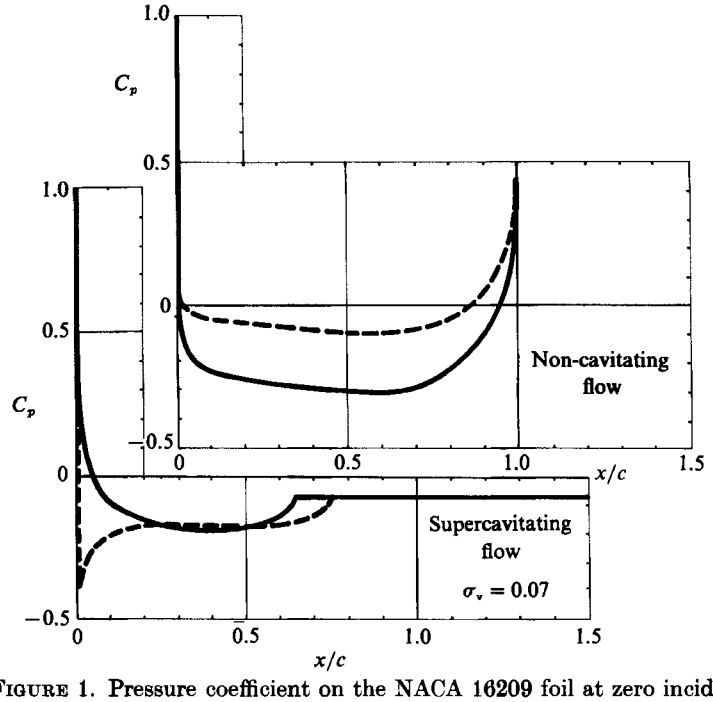

FIGURE 1. Pressure coefficient on the NACA 16209 foil at zero incidence
——, upper side; — —, lower side.

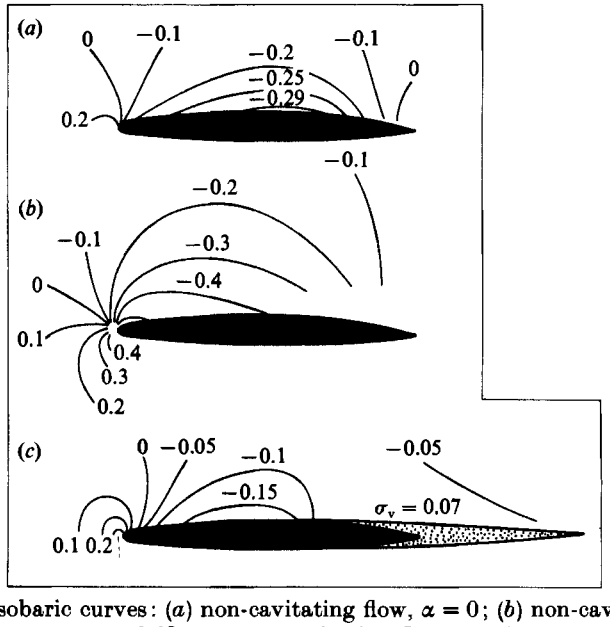

FIGURE 2. Isobaric curves: (*a*) non-cavitating flow, $\alpha = 0$; (*b*) non-cavitating flow, $\alpha = 3.2°$; (*c*) supercavitating flow, $\alpha = 0$.

The calculation of the bubble trajectories in the vicinity of the foil shows that the screening effect is noticeable for bubbles which have an initial diameter of about 1 mm. But for the cases of present concern, with a diameter range lower than 0.1 mm, we found this effect negligible. In addition the rapid films show that the velocities of the bubbles near the foil are not very different from the liquid velocity:

the slip does not exceed 10%. It can be shown that this result complies with the Hsieh equation. Thus it appears reasonable for further estimates to identify bubble paths with streamlines and to take the bubble velocity equal to the local liquid velocity.

Additional information is obtained from numerical calculations (see also Kodama *et al.* 1979). For low values of the cavitation number σ_v, defined as $\sigma_v = 2(p_r - p_v)/\rho U^2$, say $\sigma_v < 0.5$, the maximum size of the bubbles exploding near the foil upper side is found to be almost independent of their initial radius R_0: in the Rayleigh–Plesset equation, the bubble evolution is controlled, for most of the growth time, by the balance between the inertial forces and the pressure difference $p_v - p_\infty(t)$. Then, we suppose that the foil is held at a small incidence in such a way that the pressure coefficient is nearly constant and equal to its minimum value C_{pm}. The radial velocity $\dot{R}$ of an isolated bubble is given by (3) or, in non-dimensional form, by

$$\frac{\dot{R}}{U} = [\tfrac{1}{3}(-C_{pm} - \sigma_v)]^{\frac{1}{2}}. \tag{4}$$

We assume that the bubble slip velocity is zero. Thus the bubble radius at the abscissa value x measured from the starting point of the underpressure zone is

$$R(x) = \left[\frac{-C_{pm} - \sigma_v}{3(1 - C_{pm})}\right]^{\frac{1}{2}} x. \tag{5}$$

For example, at a foil incidence of 1°, $C_{pm} \approx -0.4$; taking $\sigma_v = 0.2$, we get $\dot{R}/U = 0.26$, $R/x \approx 0.22$. Those values are correct for isolated bubbles and slightly overestimated when several bubbles are present. In both cases the linear dependency between R and x agrees quite well with the bubble evolution that we have obtained in our experiment, thus giving some validity to our simplifying assumptions. Incidentally, we can also consider the more general case when a number of bubbles explode at the same time on the foil: inside the restricted framework considered through this section the λ^{-3} rule, which ensures that the relative distances between active nuclei have the same mean value, is a sufficient condition for the similarity of two cavitating flows with transient bubbles, when it is added to the usual condition on the cavitation index σ_v.

Finally we point out that, owing to the variety of initial hydrodynamical conditions in non-cavitating flows, very different cavitation patterns can be encountered in experimental work. Here we consider primarily transient bubbles and attached cavities, but other phenomena appear which cannot be clearly put in either class unless some objective features are used in order to distinguish them properly. Thus, in view of the distinction operative in experiments, it can be useful to call 'bubbles' those phenomena for which the relative liquid velocity is mainly normal to the interface, while the term 'cavity' is suitable if the relative velocities are mainly tangential to the interface, but without creating circulation, however, contrary to cavitating vortices.

3. Experimental set-up and methods

The tests were carried out in the second free-surface channel of the hydrodynamic tunnel at Grenoble University (Briançon-Marjollet & Michel 1987). The test section is 1.6 m long, 0.12 m wide and 0.40 m high. The absolute pressure p_0 at the free surface of the channel can be lowered to a value close to the vapour pressure

p_v while the free-stream velocity U is in the range 2.5–13.0 m/s. The submersion depth of the body is $h = 0.20$ m. Thus the cavitation index σ_v is expressed as $\sigma_v = 2(p_0 + \rho gh - p_v)/\rho U^2$; it can be lowered to the limit value 0.07 in the present experiments. The low value of the ambient pressure tends to reduce the concentration of dissolved air in water to less than 2 p.p.m. The free-stream turbulence intensity varies from 0.12 to 0.16 % when U varies from 3 to 12 m/s, except along the Plexiglas sidewalls where the boundary-layer thickness is about 1.5 cm. The NACA 16209 hydrofoil is cambered by 2 %, its relative thickness is 9 % and its chord c is 0.10 m, so that the Reynolds number $Re = Uc/\nu$ is in the range 0.25×10^6–1.3×10^6. Experience shows that, in that range, the Reynolds number does not have a strong influence, thus the major part of the results presented here correspond to $U \approx 10$ m/s, $Re \approx 10^6$. The hydrodynamic tunnel is equipped with a wall balance, and force measurements – lift, drag and pitching moment – were taken in order to characterize the dynamic response of the various cavitating flow regimes. However, the results of those global measurements are not given here because they do not provide any detailed information on the interaction mechanisms constituting the main focus of this paper. The visualization techniques which use dye injection are well suited to the analysis of the global boundary-layer behaviour. Here water coloured with fluorescein was used in the same way as in the previous studies, but three small injection holes (0.2 mm in diameter) 3 cm along the span direction, were drilled on the foil leading edge. Several rapid films (5500 images per s) and numerous photographs were necessary to demonstrate the typical events of the bubble–boundary layer interaction, as their probability of occurrence above the coloured threads could be weak. In some cases, conical supercavitation arose from the injection holes, which made it necessary to machine a second foil. Both foils are seen on the various photographs shown in the paper. The photograph on figure 3 shows laminar separation of the boundary layer in non-cavitating flow, which is the reference case for both cavitation regimes: attached cavity or transient bubbles.

We now proceed to describe the essential features of the nuclei control system, a detailed description and valuation of which are given by Briançon-Marjollet (1987). The system was studied by Lecoffre and Marcoz at the ALSTHOM–A.C.B.–C.E.R.G. Company (Lecoffre 1987). The generation of nuclei comes from supersaturated water which is injected into the tunnel through small orifices. Owing to the design of the injectors, small supercavities are created which release a large number of tiny bubbles. The injection system is located about 4 m upstream of the tunnel test section and the residence time of the nuclei does not exceed 4 s when the free-stream velocity U is 10 m/s. Thus the decanting of nuclei by gravity is small and the air exchange between the nuclei and the surrounding water is negligible. Also, such nuclei are fresh and their superficial tension is not modified by water impurities, so that the Rayleigh–Plesset model can be used with some confidence. The maximum production rate of nuclei is about 5×10^6 per s, which gives a concentration equal to 10 nuclei per cm^3 when the free-stream velocity is 10 m/s. A second injection line allows us to decrease the nuclei seeding by means of one injector only which is set up in a dilution chamber. The dispersion of the nuclei is not fully achieved at the test section entry and both cavitating regimes can be juxtaposed on the hydrofoil upper side (figure 4, plate 1). We observe that the corresponding pressure distributions are matched through a small thickness in the spanwise direction.

The measurement of the nuclei population uses the stability criterion of isolated nuclei, see equation (1) (Oldenziel 1979). The present counting device is made up of three main elements. First, a venturi throat is followed by a rapidly diverging cone

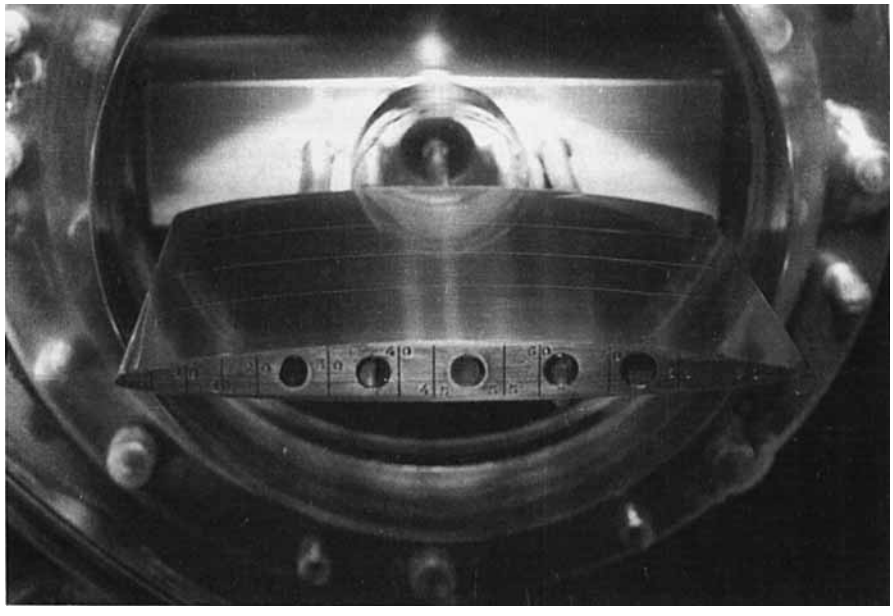

FIGURE 3. The basic non-cavitating flow at $\alpha = 0$, with laminar separation near the trailing edge.

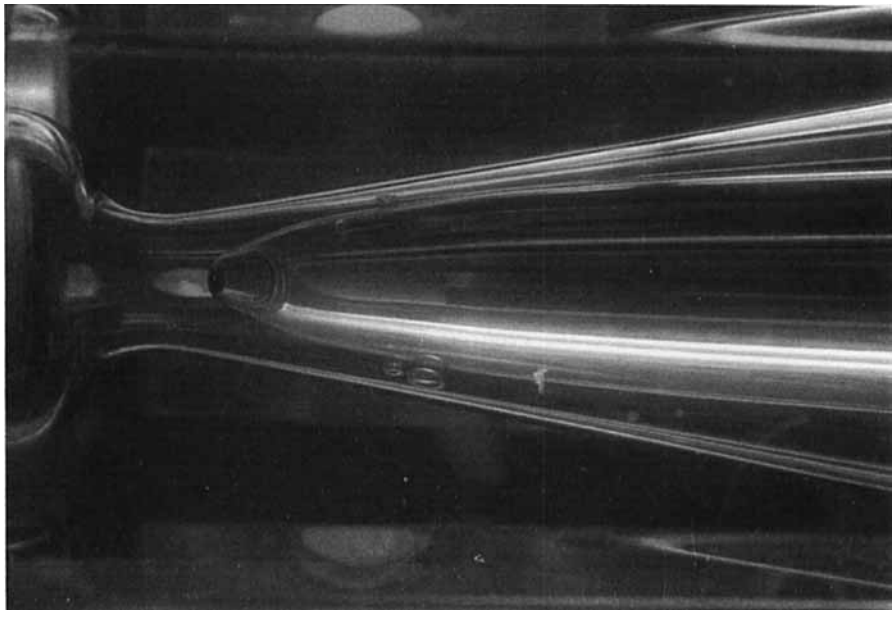

FIGURE 5. Bubble explosion in the ogive–venturi counter at rate of 1044 nuclei per second.

in which an ogive is placed (figure 5). There the nuclei undergo a sudden underpressure followed by a smooth pressure distribution, with a minimum value p_n at the narrowest cross-section, the area of which is about 62 mm^2. Second, the bubbles which explode in that region are counted by a piezo-electrical ceramic which picks up the noise they emit when imploding downstream. Finally, the venturi is

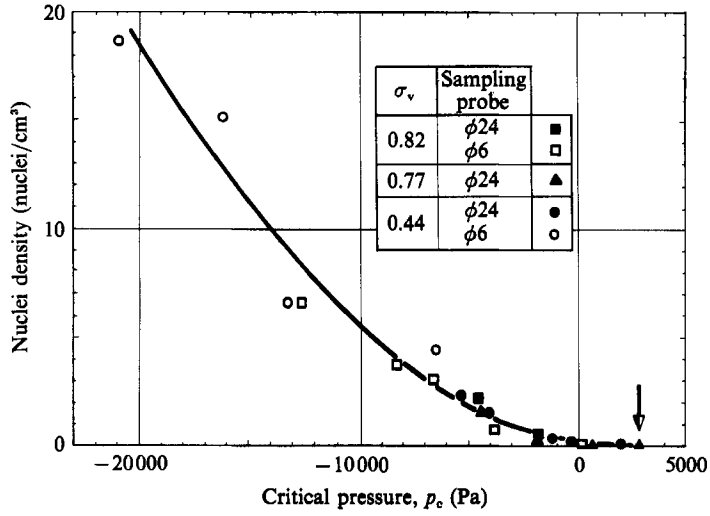

FIGURE 6. Cumulative histogram of the nuclei population at velocity 9.8 m/s.

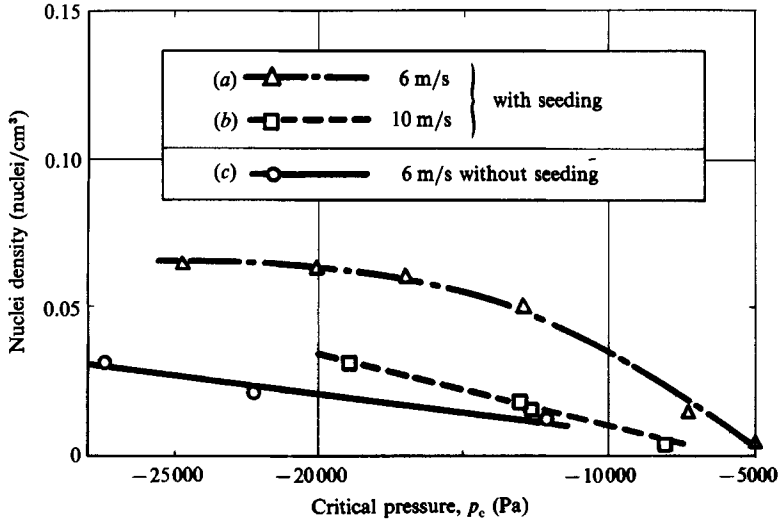

FIGURE 7. Nuclei recirculation in the hydrodynamic tunnel at atmospheric pressure.

supplied with sampled water through two lines (respectively 24 and 6 mm in diameter), the second one using a dilution chamber in order to avoid saturation of the ogive by cavitation for the high nuclei concentrations. The sampling probes are located about 1 m upstream of the tunnel test section. The maximum flow rate is about 1 l/s and the maximum counting rate about 1800 events per s; by means of dilution, concentrations as high as 20 nuclei per cm^3 can be measured. The results of those measurements are presented as cumulative histograms: the ordinate is the number of nuclei per cm^3 whose critical pressure is greater than or equal to the abscissa $p_c, p_c = p_n$. Note that each experimental point results from the examination of large sampled volumes, up to 0.1 m^3. The actual nuclei evolution through the venturi meter is dynamical in nature and, as a result, the minimum pressure p_n is not exactly the critical pressure of the smallest nuclei which explode in the ogive–cone duct. However, it can be shown that the design of the duct reduces the expected

difference to a negligible value, especially in comparison with the experimental errors. Figure 6 shows typical cumulative histograms corresponding to the case of flow thought to be fully seeded with nuclei. By comparison with figure 6, the ordinate scale in figure 7 shows that the nuclei recirculation in the hydrodynamic tunnel is low, if seeding is carried out (see cases *a* and *b*); if not, only a few nuclei are present (see case *c*). Their number is even smaller and their critical pressure lower than about -25000 Pa when the reference pressure p_0 is reduced to a value close to the vapour pressure.

From the viewpoint of cavitation inception, the largest value p_s of the abscissa p_c in the cumulative histogram – the liquid susceptibility (Lecoffre & Bonnin 1979) – is of interest since it corresponds to the weakest points in the liquid continuum. In practice, the hydrodynamical tunnel and the nuclei generator are such that two kinds of nuclei populations are produced: without any nuclei seeding the susceptibility is low, as in case (*c*) of figure 7; with nuclei seeding, the susceptibility is in a narrow range, from about -4000 Pa to a value close to the vapour pressure, because the size of the largest nuclei is almost independent of the nuclei production rate. That point must be borne in mind as some experimental results that we shall present hereafter are marked by the actual nuclei population and must be properly interpreted.

A last point deserves further comments. Compared to the present dynamical method, optical methods usually give concentrations of counted objects which are larger by one or several orders of magnitude. Thus the validity of the present measurements may appear questionable. The following procedure is used to settle the question. First, from nuclei counting it is possible to roughly estimate the number of bubbles that are likely to explode in the vicinity of the foil, if we take into account the mapping of the flow by isobaric curves (figure 2). Second, the analysis of rapid films gives the number of bubbles which actually explode in that region. For two flow configurations differing in the foil incidence and the cavitation number, the ratios of the estimated numbers to the actual ones are found to equal 0.5 and 2.5. That result shows that the present nuclei counting technique is sufficiently accurate with respect to the population of active nuclei. Finally we note that, when optical methods discriminate between microbubbles and particles, they measure nuclei concentrations in sea water close to the populations produced and measured by the present nuclei control system (O'Hern, d'Agostino & Acosta 1988).

4. Experimental results without nuclei seeding

The basic behaviour of the boundary layer on the foil upper side in the non-cavitating regime is shown in figure 8. The boundary layer is calculated by the integral method devised at ONERA by Arnal, Habiballah & Coustols in 1984. The agreement between experimental and numerical results is good for the position of laminar separation; the sudden upstream motion of the transition region at an incidence of about 2.5° is well described by the numerical method. In the case – not shown here – of a Reynolds number equal to 6×10^5, the transition curves are shifted by roughly 1° towards the largest angles of attack.

The various flow patterns and the corresponding domains in the (α, σ_v)-plane are sketched on figure 9. The general behaviour of the cavitating flow resembles that described in FM (1985) for a symmetrical NACA 16012 hydrofoil. Domain 1 is non-cavitating. Cavity detachment is on the whole two-dimensional in domain 2 and it takes place at the rear part of the foil. Then it moves upstream and becomes three-

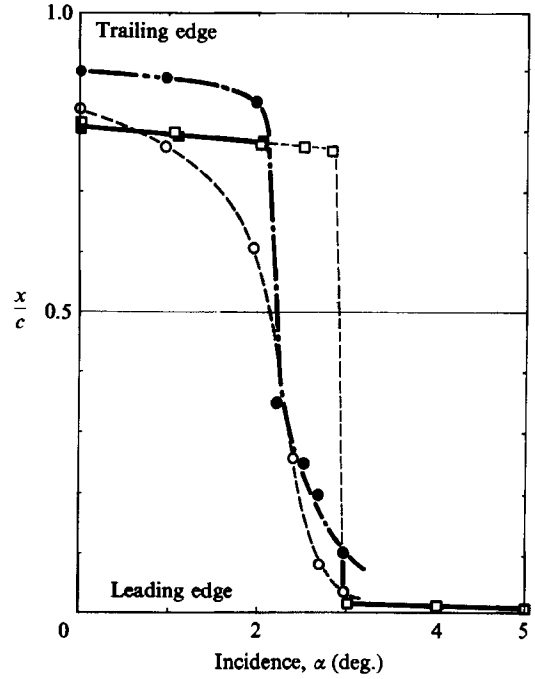

FIGURE 8. Behaviour of the boundary layer in non-cavitating flow at $Re = 10^6$. Laminar separation: □, calculations; ■, experiments. Start of transition to turbulence with $Tu = 0.16\%$: ○, calculations; ●, experiments.

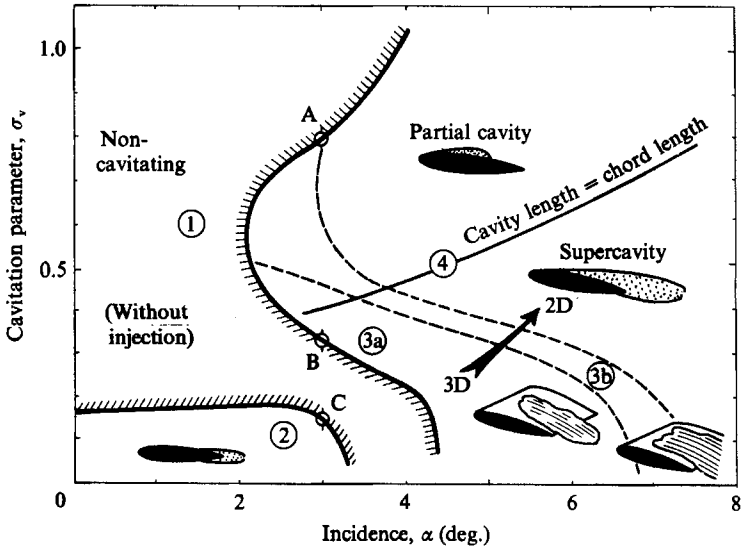

FIGURE 9. Attached-cavitation patterns, $Re = 10^6$.

dimensional in domain 3, while its transverse scale decreases when domain 4 is approached. There the cavity starts from the leading edge and the two-dimensional character of detachment is found again.

In figure 9, the frontier between the cavitating and non-cavitating regimes was obtained, the cavitation number remaining constant, by increasing the angle of

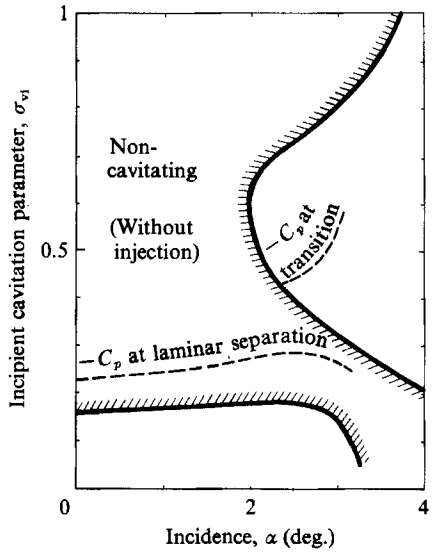

FIGURE 12. Measured σ_{vi}-curve and calculated $|-C_p|$-curve, $Re = 10^6$.

attack. As expected, some hysteresis is found when the experimental path in the (α, σ_v)-plane is changed, for instance with a fixed incidence and a variable reference pressure. However, the S-shaped interface between domain 1 and domains 3, 4 is well established, although disconcerting. It is even more marked than in the previous study since, with a 3° attack angle a small cavity can appear at the leading edge for $\sigma_v \approx 0.79$ (point A on figure 9) then disappear at B for $\sigma_v \approx 0.32$ and finally reappear at the downstream part of the foil for $\sigma_v \approx 0.15$ (point C). Figure 10 (plate 2) shows some stages of cavity evolution. Here incipient cavitation at the leading edge takes the form of isolated conical cavities while in approximately identical conditions the NACA 16012 hydrofoil produces a rather large two-dimensional cavity, which explodes at inception for $\sigma_v \approx 0.50$ (figure 11, plate 1). The difference may be due to local conditions – roughness and curvature of the leading edge – but it does not affect the general shape of the interface in the (α, σ_v)-plane.

In the non-cavitating regimes neighbouring cavitation inception at points A and C on one side and point B on the other side, the global hydrodynamic conditions are identical as far as distribution of the pressure coefficient, boundary-layer behaviour, transition to turbulence, intermittency and pressure fluctuations are concerned. Figure 12 shows the absolute values of the calculated pressure coefficient either at laminar separation in non-cavitating flow or at the calculated transition points. For the leading-edge cavities, i.e. the region of point A in figure 9, incipient cavitation seems to be connected to the turbulent pressure fluctuations in the transition region, which can reach 20% of the dynamical term $\frac{1}{2}\rho U^2$ (Huang & Peterson 1976). For downstream cavities, the σ_{vi}-curve, where σ_{vi} stands for the value of σ_v at inception, is rather close to – and lower than – the $|C_p|$-curve at separation. Most of the difference is due to the adverse pressure gradient since cavity detachment takes place downstream of laminar separation. It must be also noted that intermittency allows the cavity to appear at the rear of the foil, which would be impossible with a steady attached turbulent boundary layer. Thus the cavitation patterns at A and C on figure 9 are predicted by two different criteria among those proposed by Arakeri & Acosta (1981) on condition that they are completed by the following requirement: to be

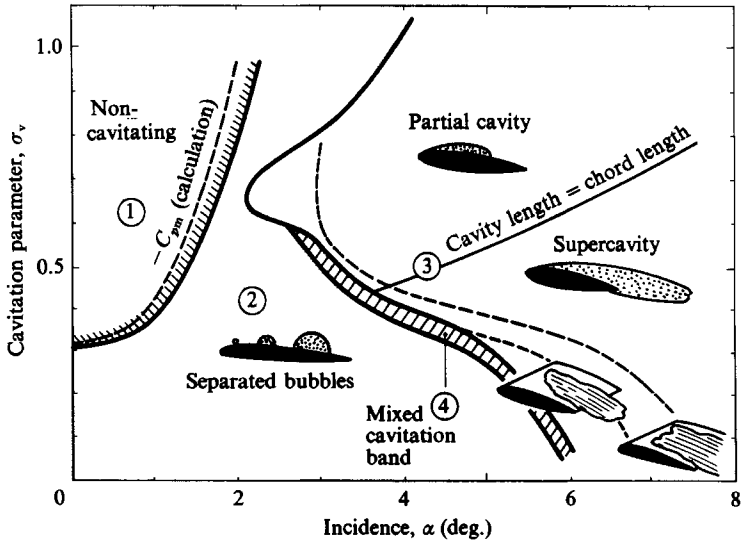

FIGURE 13. Cavitation patterns for full nuclei injection, $Re = 10^6$.

stable, an attached cavity must be accompanied by a pressure distribution creating laminar separation before its detachment. Even with that restriction, the branching of the flow to either configuration is not fully understood. As a conjecture we can imagine that some transient attempts are made by the flow to get over the cavitation threshold. A possibility can be provided by the explosive growth of a number of nuclei in the transition region. Unattached, flat cavities, which can actually be observed under stroboscopic lighting in the case of the largest flow velocities, are an alternative for the smaller values of the ambient pressure. We shall see that such transient cavities can be created by explosive bubbles, as a result of their interaction with the boundary layer.

5. Global results with a variable nuclei concentration

Now we consider the case when the nuclei population in water is enriched by means of the nuclei control system. First we examine the effect of a full injection, the nuclei generator operating at its maximum rate. Different cavitation patterns are then obtained according to the foil incidence and the value of the cavitation number. The corresponding domains in the (α, σ_v)-plane are shown in figure 13. For large angles of attack, the leading-edge cavities are not affected by the added nuclei. On the other hand, at low incidence, cavities are replaced by transient bubbles (figure 14, plate 3) and, as expected, the domain of the cavitating regime is enlarged. Between those domains, we find a mixed cavitation band in which transient bubbles alternate with cavities or are simultaneously present with them on a part of the foil (figure 15, plate 3). It is noticeable that the limit of the nuclei effectiveness coincides quite well with the limit of the two-dimensional, leading-edge cavity domain, i.e. domain 4 in figure 9. Thus it can be inferred that this limit does not depend on the maximum production rate of the nuclei generator: this will become clearer in due course. When the concentration of nuclei in the water is reduced, the mixed cavitation domain expands to the left of the figure to the detriment of the transient-bubble regime.

In figure 13, the domain of nuclei activity for the low incidences is limited by a

σ_{vi}-curve which is close to the $|C_{pm}|$-curve, where C_{pm} is the minimum pressure coefficient. Conventionally, the conditions of incipient cavitation correspond to observable bubbles with a maximum diameter of about 1 mm, appearing at a rate of about one per second. Those incipient cavitation figures are close to the point of minimum pressure. When the flow velocity is decreased, the difference $|C_{pm}|-\sigma_{vi}$ increases. Owing to the above-mentioned narrowness of the liquid susceptibility range produced by the nuclei seeding system, the conditions of incipient cavitation cannot be varied to a large extent in the present experiments and thus only the main tendencies can be presented. They agree fairly well with the rule of equality between the liquid susceptibility p_s and the minimum pressure p_m at the bubble cavitation threshold (see for instance Lecoffre & Bonnin 1979; Keller 1984), or in non-dimensional form:

$$(\sigma_{vi})_{bubbles} = |C_{pm}| - \frac{p_v - p_s}{\frac{1}{2}\rho U^2}.$$

Using that rule as a guide, we look for the susceptibility that should be required in order to replace an attached cavity by transient-bubble cavitation at the low foil incidences. With the following values: $C_{pm} = -0.302$ ($\alpha = 0$), $U = 10$ m/s, and $(\sigma_v)_{cavity} \approx 0.16$, we find $p_s \approx -5000$ Pa. That value is far above the tunnel water susceptibility which, as was already mentioned, does not exceed -25000 Pa at the low pressures required by the experiments. Conversely, thanks to other experiments carried out with a roughly streamlined body, it was checked that transient-bubble cavitation can appear in that strongly deaerated water at the following value of the cavitation number: $\sigma_{vi} \approx 0.45$. From the above equation, that is possible if $|C_{pm}| \approx 1.0$, which is the order given by calculations for that body. However, we must bear in mind, with reference to the delay needed by the bubble growth, that the minimum pressure region should not reduce to a narrow peak but has to spread out over a significant part of the foil.

The photographs presented in this paper show a large variety of bubble shapes. Roughly speaking, we can distinguish the bubbles that intersect the foil surface – for convenience, they will be called half-bubbles – from the others, although nothing can be said on the conditions to be fulfilled by the original nuclei in order to generate either shape. Note in figure 23 that the bubble whose image is visible has a size of about 13 mm, while the distance from its centre to the foil is about 11 mm; however, it is not far from a spherical shape. From the viewpoint of interaction between the bubbles and the boundary layer, half-bubbles are more effective since they disturb the foil pressure distribution in a steeper way. It happens that, for the small incidences we consider here, they maintain their spherical shape fairly well during their explosion, even if several bubbles are present. That is the reason why we adopt rather coarse approximations in §2. Both kinds of bubbles are deformed by the pressure gradient which compels the interface to involve and initiate a re-entrant jet, as in figure 14 or to be elongated (figure 16, plate 4). A question arises concerning the half-bubble base, i.e. that part of the bubble in contact with the foil: is it dry or does a thin water film exist under the bubble? When studying the photographs we incline to the second solution. In particular, the water film can explain that iridescences are seen under several half-bubbles: they could be due to the initial turbulent state of the boundary layer.

The last point to be examined in this section is related to the saturation of the downstream part of the foil by the transient bubbles. The phenomenon occurs – see figure 17 (plate 4) – when the bubbles grow and join by their bases at the abscissa point x_S. Later on, they grow mainly in the y-direction before coalescing more or less

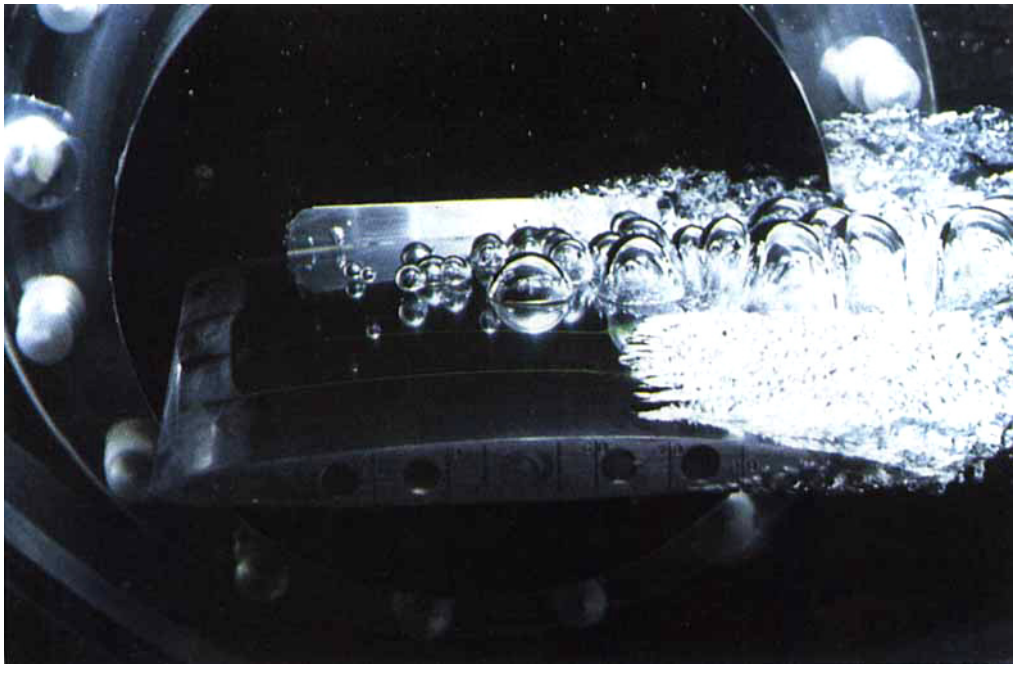

FIGURE 4. Cavity flow and transient bubble flow: $\sigma_v=0.08$, $\alpha=1.5°$.

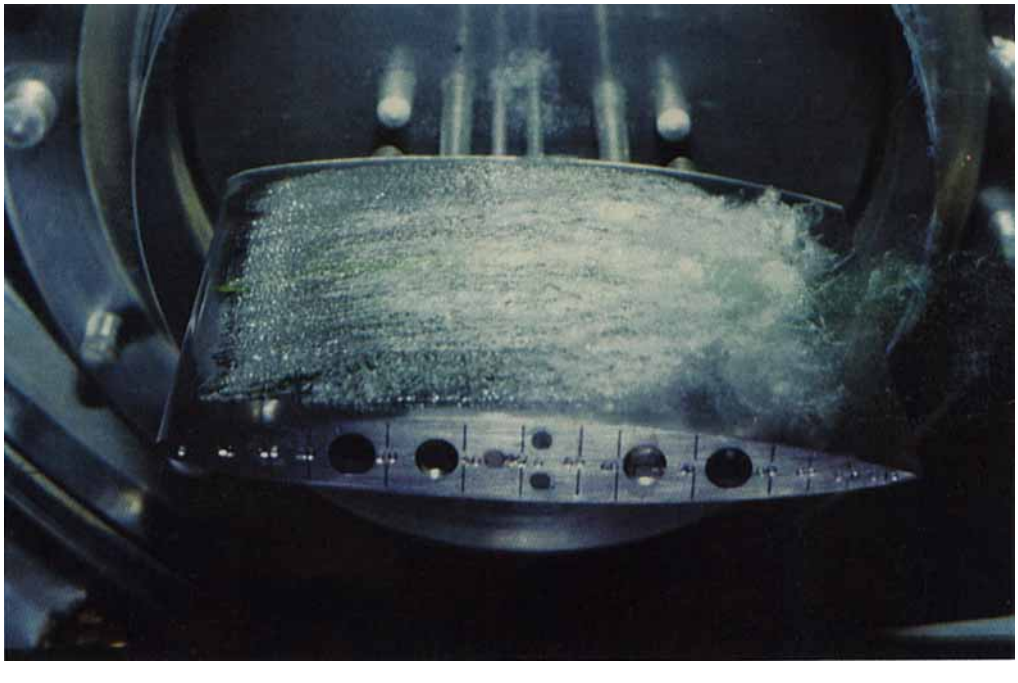

FIGURE 11. Cavity inception on a NACA 16012 hydrofoil near point A of figure 9. $Re=10^6$, $\sigma_v=0.49$, $\alpha=4°$.

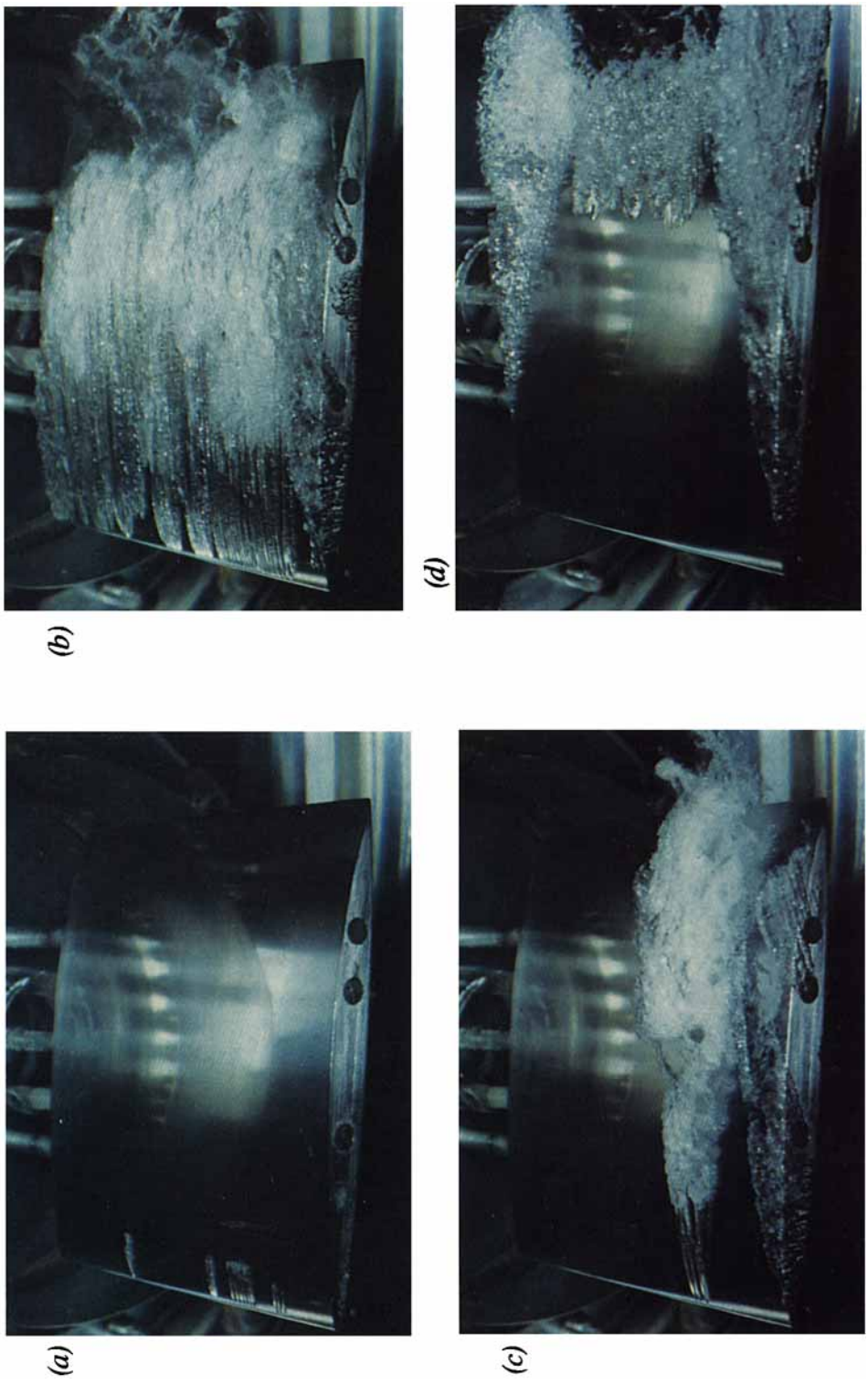

FIGURE 10. Cavity evolution for a decreasing σ_v, $Re=10^6$, $\alpha=3°$. *(a)* $\sigma_v=0.79$; *(b)* $\sigma_v=0.52$; *(c)* $\sigma_v=0.34$; *(d)* $\sigma_v=0.14$.

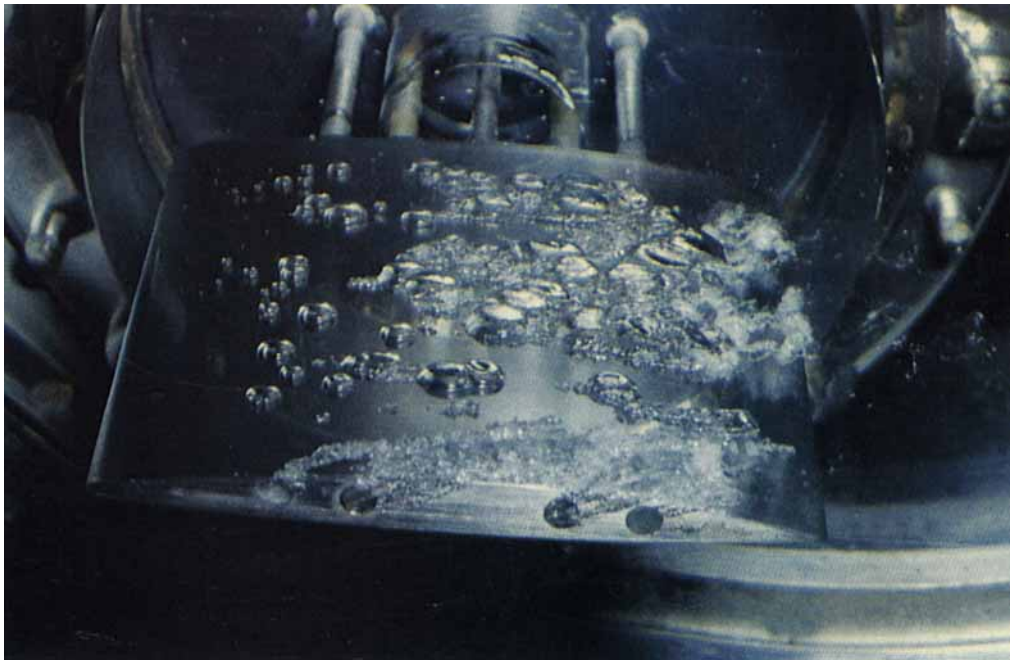

FIGURE 14. Transient bubble flow. $Re=1.3\times10^6$, $\sigma_v=0.29$; $\alpha=2°$. Domain 2 of figure 13.

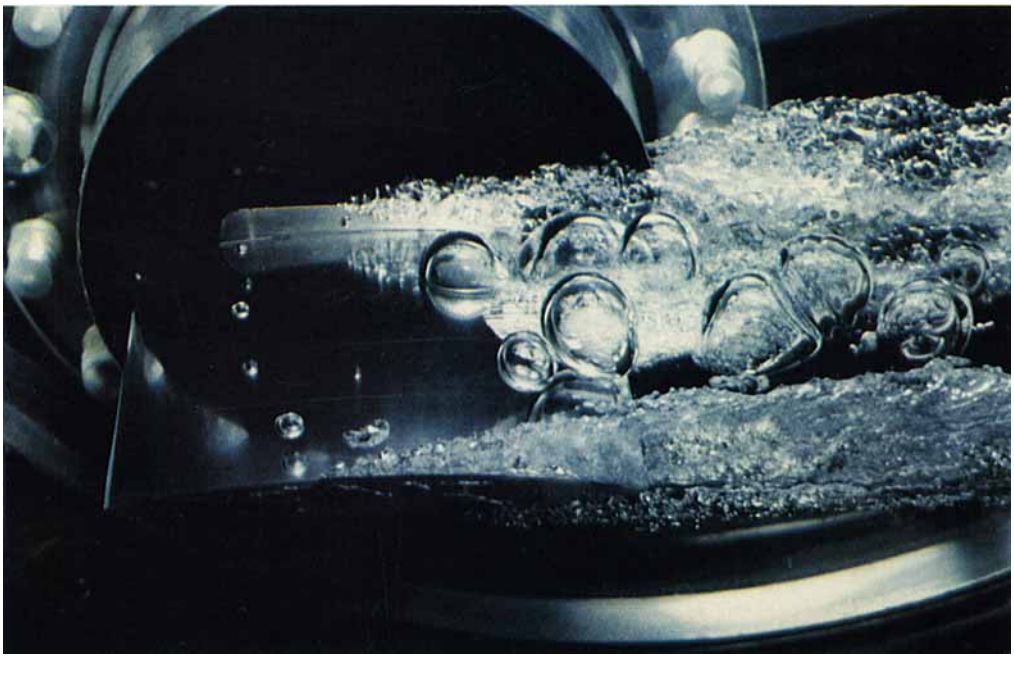

FIGURE 15. Mixed cavitation regime. $Re=10^6$, $\sigma_v=0.07$; $\alpha=1.1°$. Partial injection of nuclei.

FIGURE 16. Non-spherical half-bubbles. $Re=10^6$, $\sigma_v=0.10$, $\alpha=5°$.

FIGURE 17. Saturation. $Re=1.1\times10^6$, $\sigma_v=0.08$, $\alpha=5°$.

FIGURE 20. Exploding bubble with an upstream transient cavity. $Re=10^6$, $\sigma_v=0.23$, $\alpha=3°$.

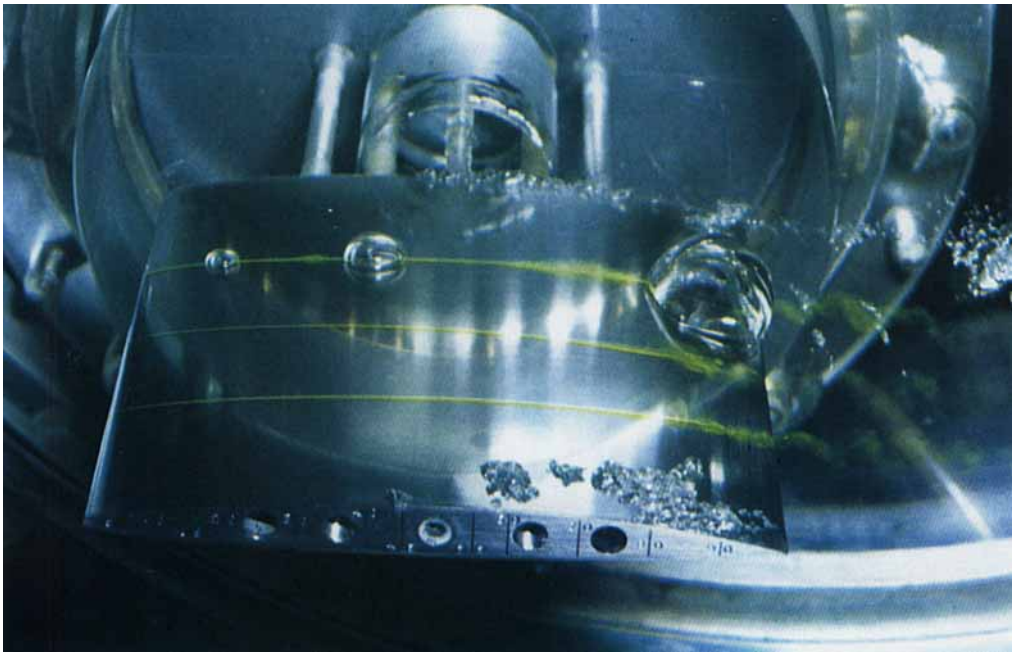

FIGURE 21. Excitation of transition to turbulence by exploding bubbles. $Re=6\times10^5$, $\sigma_v=0.20$, $\alpha=1°$.

FIGURE 22. $Re=10^6$, $\sigma_v=0.09$, $\alpha=1°$.

FIGURE 23. Sweeping away of a part of the rear cavity by a turbulent spot. $Re=10^6$, $\sigma_v=0.09$, $\alpha=1°$.

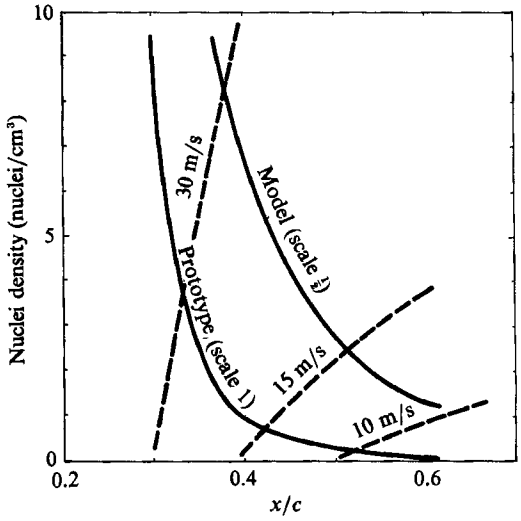

FIGURE 18. Evaluation of the saturation abscissa x_S: ——, active nucleus density required for saturation at x; – – –, active nucleus density available if saturation is at x.

into an almost continuous cavity. Let us consider R_S as the base radius of those bubbles. The surface density n' of bubbles in the saturated region is approximately $\frac{1}{4}R_S^2$. Then the required concentration n_S of nuclei that are destabilized in the upstream region through the liquid layer, whose thickness is δ, is given by

$$n_S = \frac{n'}{\delta} = \frac{1}{4R_S^2\delta}. \tag{6}$$

Such an expression obviously contains the similarity law λ^{-3} through the dimension of the concentration itself. For a further estimate, we need some simplifying assumptions: in the saturated region, the pressure is the vapour pressure p_v and upstream of it the pressure distribution is calculated by a cavity model which does not include the presence of isolated bubbles. For the small incidences we have in mind, we assume the pressure to be almost constant: $p \approx p_m$, where p_m is the minimum value; the bubble radius R_S can then be estimated by expression (6), corrected by a coefficient k in order to take the neighbouring bubbles into account. For instance, with $\sigma_v = 0.07$, $x_S = 60$ mm ($\alpha = 0°$), we have $C_{pm} \approx -0.168$; taking $k = 0.8$, we find $R_S \approx 8$ mm, while the experimental value given in that case by the photographs is 7.5 mm. The estimate of the thickness δ in (6) is a more difficult problem. A first possibility is to take the maximum distance from the isobaric curve $p = p_v$ to the foil – that value can be also approached by means of the Euler equation – which gives $\delta \approx 19$ mm. Obviously this is too thick because, actually, the bubbles that grow near the foil prevent the external nuclei from exploding. Another possibility is to look at the boundary-layer thicknesses, but no sound basis is available for this. Thus we prefer to evaluate δ from the rapid films, which give $\delta \approx 2$ mm, with a possible important error nevertheless. Then in (6) we find $n \approx 2$ nuclei/cm^3, which is the experimental value. An attempt to describe the modification of the pressure field by bubbles was made by Menoret & Blayo (1988). In the present approach, the δ-value might increase slightly when σ_v decreases, while the k-value might decrease when a large value of n is expected, i.e. for small values of x_S. However that may be, the transverse coordinate is likely to play a role different

from the foil surface coordinates: then the exponent in the similarity law could be lower than 3 but larger than 2.

From fundamental and practical viewpoints, it is useful to know the values x_S and n_S of the actual flow when the governing parameters Re, α, σ_v are given together with the nucleus population in water. The point (x_S, n_S) is found at the intersection of the $n_S(x_S)$-curve given by (6), which represents the required number of active nuclei, with the $n_a(x_S)$-curve resulting from the nuclei histogram and the minimum pressure upstream of x_S. For that estimate we take $k = 1$, $\delta = 2$ mm. In figure 18, besides the present configuration, we consider an hypothetical prototype flow with a scale factor $\lambda = 2$ and an identical nucleus population. In practice, for the high velocities, the relative x_S/c tend to a limit for each configuration and the similarity law becomes useless. That can be related to the limited effect of high nucleus concentrations as pointed out by Avellan *et al.* (1986) as already mentioned. In the limit state, the flow can be called fully saturated by bubbles.

6. Interactions

Now we pay further attention to the mixed cavitation regime, already described in brief in §5. The main question is: how do the bubbles sweep a pre-existent cavity away? Obviously, it implies an insight into the local interactions between the ingredients we have at our disposal: bubbles, cavities, and the boundary layer.

The interaction between an attached cavity and the boundary layer is considered in some detail in FM (1985). It calls into play the pressure-gradient distribution whose function is twofold: first, by integration from a reference point to the cavity detachment, it results in the vapour pressure value; secondly, it controls the laminar boundary-layer development so that separation takes place just upstream of cavity detachment. The conclusion still holds in the case of unsteady flows, namely flows around a hydrofoil oscillating in incidence (FM 1988), for frequencies as high as 21 Hz; the corresponding time is less than 0.05 s, a value not too far from the present bubble convection time c/U, $c/U \approx 0.01$ s for $U = 10$ m/s. Thus, when considering interactions of explosive travelling bubbles with an attached cavity and the boundary layer, we are led to look first at the unsteady disturbances that the bubbles bring to the foil pressure distribution. For a hemispherical bubble, we expect a maximum pressure along the base perimeter and a zero perturbation at some distance from the bubble centre. Detailed calculations on this are given by Briançon-Marjollet (1987), taking the longitudinal pressure gradient of a basic one-dimensional, non-viscous flow into account, and assuming the spherical symmetry of the explosive bubbles, see figure 19. If one neglects the bubble slip velocity and the growing acceleration $\ddot{R}$, the overpressures at downstream and upstream points A and B are

$$\frac{\Delta p_A}{\rho} \approx \tfrac{3}{2}\dot{R}^2 + [U(x_0) - U(x_0 + R)]\dot{R},$$

$$\frac{\Delta p_B}{\rho} \approx \tfrac{3}{2}\dot{R}^2 - [U(x_0) - U(x_0 - R)]\dot{R},$$

where $U(x_0)$ is the basic velocity at the bubble centre abscissa. In these expressions, the first term $\frac{3}{2}\rho\dot{R}^2$ is dominant, especially if the basic pressure gradient is low. Then relation (5) gives

$$\Delta p_A \approx \Delta p_B \approx \tfrac{1}{2}\rho U^2(-C_{pm} - \sigma_v),$$

which allows us to find the expected vapour pressure value at points A and B and

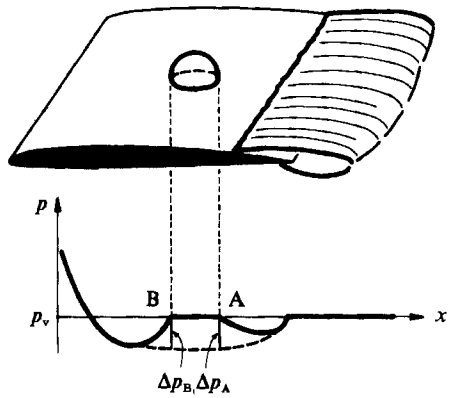

FIGURE 19. Sketch for the calculation of the bubble overpressure.

conclude that the model is consistent, on the whole. At a $2R$ distance from the bubble centre in the streamwise direction, the overpressure is about $\rho\dot{R}^2$ so that the overpressure gradient is at least $\rho\dot{R}^2/2R$ in the bubble vicinity.

The effects of that travelling overpressure are now examined by an *a priori* reasoning which leads us to consider several possible scenarii for the sweeping away of an attached cavity by transient explosive bubbles:

(i) At a fixed point downstream of it, the oncoming bubble produces an increasing pressure at a temporal rate

$$\frac{\partial p}{\partial t} \approx \frac{\rho\dot{R}^2}{2R}[U(x_0)+\dot{R}].$$

If we take expressions (4) and (5) into account, we find

$$\frac{\partial p}{\partial t} \approx \frac{\rho\dot{R}^3}{2R^2}\left(1+\frac{R}{x_0}\right)$$

and, with $C_{pm} \approx -0.4$, $\sigma_v = 0.2$, $U \approx 10$ m/s, $x_0 = 5$ cm, we obtain, as in §2, $\dot{R}/U \approx 0.26$, $R/x_0 = 0.22$, which results in $\partial p/\partial t \approx 4.4 \times 10^6$ Pa/s. That value is considerable since the pressure at the fixed point is increased by 4400 Pa in 1 ms, the time needed for the motion of the bubble over one radius, while the water vapour pressure is in the range 1700–2300 Pa at room temperature. As a possible event, that sudden blast could be strong enough to destroy the mechanical equilibrium at detachment and to suppress the cavity. The outcome is not clear, however, because the available time is short and then the total impulse can be low. Also, when the bubble approaches the cavity detachment point, its maximum overpressure decreases with $-C_p$, according to our previous estimate, and ultimately the two regions where pressure is p_v become superposed.

(ii) Another possibility is the reduction of the basic adverse pressure gradient in the downstream region. It may result in the disappearance of the boundary-layer laminar separation and thus lead to cavity suppression.

In the region located upstream of the bubble, the unsteady pressure distribution tends to increase the spatial distribution of the basic adverse pressure gradient. Thus we can expect the following primary effects:

(iii) the appearance of a new laminar separation,

(iv) the excitation of transition to turbulence into the boundary layer.

Scenarii (i) and (ii), should they occur, would not be easily identified. In fact, the

direct suppression of a cavity by an oncoming bubble is not observed in our experiments. Instead of that, it fairly often happens that half-bubbles pass over the cavity detachment without bringing any visible disturbance to the cavity. Note that descriptions of such sequential events are possible from rapid films only, while the photographs displayed in this paper only aim to illustrate the phenomena.

The appearance of a new laminar separation upstream of an explosive bubble is not directly observed in our experiments. It is, rather, inferred from cavitation patterns such as the one shown on the photograph of figure 20 (plate 5) for which unfortunately no rapid film is available: the bubble is accompanied, on its upstream side, by a travelling vapour pocket whose general aspect is closer to a cavity than a bubble. In particular its flatness seems to indicate large tangential relative liquid velocities on the major part of it, although important normal velocities on the cavity sides can be suspected if laminar separation actually shelters the cavitating region. Whatever the interpretation may be, that cavitating phenomenon results from the interaction between bubbles and the boundary layer. As mentioned in §4, it offers a possible mechanism for the passage of the cavitation threshold to the attached-cavity regime.

In some respects exploding bubbles resemble the artificial puffs that aerodynamicists inject into boundary layers in order to study the flow stability and associated topics. In the same way, the pressure field surrounding bubbles can destabilize the boundary layer and generate the conditions of transition to turbulence. Turbulent spots are seen upstream of two half-bubbles above a coloured thread in figure 21 (plate 5). As a counterpart, the lateral effect of bubbles in the spanwise direction seems usually to be weak, as shown in figure 22 (plate 6). The destabilizing effect is not expected downstream of the bubble. Indeed, it is never observed there.

The first global effect of turbulence is to delay the separation of the boundary layer. Thus laminar separation is destroyed every time a turbulent spot reaches it. As a consequence, an attached cavity must also be temporarily suppressed by the turbulent spot a bubble is able to create. That conclusion is effectively supported by the observation of several films from which we retain about ten crucial events, i.e. those events in which the following sequence clearly appears: the growth of a half-bubble above a coloured thread, the development of a turbulent spot, the passage of the bubble over the cavity detachment without cavity disturbance and finally the sweeping away of the cavity by the turbulent spot. That last stage is produced as soon as the spot reaches the detachment point, without any perceptible delay or change in the spot length, so that its characteristic time is lower than 10^{-4} s. Figure 23 (plate 6) shows the final stage of the sequence for the half-bubble seen on the right-hand side of the midspan, riding a piece of cavity which has previously been detached from the foil by the turbulent spot generated by the half-bubble itself. The other two bubbles which appear almost spherical in figure 23 do not influence the cavity. To illustrate this phenomenon, it can be said that bubbles do not push the cavity, but they pull it via transition to turbulence in the boundary layer.

After a part of the cavity and the turbulent spot have been carried away by the flow, laminar separation and a new cavity appear, if no other bubble excites the boundary layer. Thus we have the following conditions for permanent cavity suppression:

(i) the pressure distribution must destabilize the nuclei present in the liquid flow,

(ii) the resulting explosive half-bubbles must excitate transition to turbulence into the boundary layer,

(iii) The rate of passage of half-bubbles at a given position in the spanwise direction must be sufficient to prevent laminar separation and cavity detachment from reappearing on the solid wall.

The last condition leads us to evaluate the time required for the restoration of laminar separation. From the films, a time T_1 is measured, of the order 10 to 20 ms, for a detachment abscissa x_D in the range 71–83 mm and flow velocities between 6.7 and 10 m/s. Another time, say T_2, can also be defined from experience:

$$T_2 = \frac{l_T + 2d}{U},$$

where l_T is the length of the turbulent spot ($l_T \approx 15$ to 20 mm), d is the distance from the cavity detachment to the foil trailing edge: $d = c - x_D$. The coefficient 2 approximately takes into account the re-establishment of cavity detachment from the trailing edge. Times T_1 and T_2 are of the same order of magnitude, but with a slightly smaller value of T_2, the ratio T_1/T_2 being between 1.2 and 2.2. For convenience, we use T_2 for estimating the active nucleus concentration required for permanent cavity disappearance. We compare the time between the passages of two consecutive bubbles, in a $2R(x_D)$ wide strip and at a given transverse abscissa, with time T_2:

$$\frac{1}{2R(x_D)\,\delta U n} \leqslant \frac{2d + l_T}{U}$$

or

$$n \geqslant n_c = \frac{1}{2\delta(2d + l_T)R(x_D)}. \tag{7}$$

When replacing R from (5) in (7), we see that the critical concentration n_c grows considerably when x_D is small, chiefly because of the very brief time left for bubble growth. In particular, for the leading-edge cavities pertaining to the domains of large angles of attack, the required nuclei concentration becomes excessively important in such a way that the actual effect of individual nuclei becomes negligible. Moreover, the minimum pressure coefficient is strongly affected by the presence of a cavity, which results in a lower bubble growth rate and a decrease in the concentration of active nuclei available.

Relation (7) is tested from a film showing the mixed cavitation regime established with an intermittency rate equal to about 50%. The flow conditions $\sigma_v = 0.06$, $x_D = 7.5$ cm, $C_{pm} = -0.18$, give $R(x_D) \approx 1.4$ cm. Taking $\delta = 2$ mm as in §5 and $l_T = 2$ cm, we obtain $n_c \approx 0.25$ nuclei per cm^3 from relation (7). The actual cumulative histogram gives 0.15 nuclei/cm^3 as the concentration available for the minimum pressure produced on the foil. Thus estimate (7) can be considered as fairly good.

Comparison of concentrations n_C for cavity disappearance and n_S for saturation at the same abscissa x can be made provided that the coefficient k introduced in §5 is taken into account. Relations (6) and (7) then give

$$\frac{n_C}{n_S} \approx \frac{k^2 R(x)}{d + \frac{1}{2}l_T}, \tag{8}$$

where R is estimated by relation (5). In the present experimental situations with trailing-edge cavities, the ratio is approximately in the range 0.18–0.40.

Finally we note that, among the three previous requirements for cavity suppression, the second statement remains partly unresolved, since accurate

conditions for the excitation of transition by explosive bubbles are not known. The most important influence parameter here is the turbulence rate. As it is low in our experimental situation, we expect that turbulent excitation will be rather easier in practical applications. However, we may consider situations in which transition to turbulence would not be easily triggered as a result of a very low turbulence rate. We can conjecture that in that case an increasing concentration of active nuclei would first produce saturation by bubbles at the detachment abscissa. Then, for higher concentrations, saturation would take place upstream. The resulting adverse pressure gradient, in the region ahead of saturation, would be lowered with respect to the previous attached-cavity case and would not be able to generate laminar separation. Thus, following conclusions of FM (1985), the attached cavity should disappear. In that particular case, saturation would be the ultimate mechanism for cavity suppression. A practical conclusion is that, in any case, the nuclei concentration n_S for cavity detachment – which can be easily estimated – appears as the limit value above which travelling-bubble cavitation will replace an attached cavity.

7. Concluding remarks

The interactions we consider in this paper are complex processes since explosive bubbles can generate or suppress cavities according to their primary effect on the boundary layer.

It is noticeable that the bubble overpressure, which would be expected to be thought of as a powerful blowing source, actually does not act directly against cavity detachment. Thus the strength of the link between cavity detachment and laminar separation of the boundary layer, previously emphasized in FM (1985) for steady flows and in FM (1988) for unsteady flows, appears more clearly. The presence of nuclei which decrease the liquid tensile strength has no effect on the conclusion. If numerous enough, bubbles can only prevent laminar separation from occurring by a change in the pressure gradient. If not, the only way they find to sweep the cavity away is by producing turbulence which results in an unseparated boundary layer.

Finally, we note that in all the experimental cases we have considered, cavity detachment seems to be associated with laminar separation. Obviously, separation is necessary for the geometrical implantation and the mechanical equilibrium of the cavity. Is laminar separation indispensable? If a cavity arises in a turbulent separated region, does it necessarily recreate a laminar boundary layer before it? Failing contrary experimental evidence, the question remains open as long as the detailed description of the small region neighbouring the cavity detachment is not available.

This research was supported by the French 'Direction des Recherches, Etudes et Techniques' (Contract DRET 84-067). We are very indebted to Mr Lecoffre for many fruitful discussions on the paper topics.

REFERENCES

ALBRECHT, K. & BJORHEDEN, O. 1975 Cavitation testing of propellers in a free surface tunnel utilizing micro air bubble control. *Trans. ASME* I: *J. Fluids Engng* **97**, 523–532.

ARAKERI, V. H. & ACOSTA, A. J. 1973 Viscous effects in the inception of cavitation on axisymmetric bodies. *Trans. ASME* I: *J. Fluids Engng* **95**, 519–527.

ARAKERI, V. H. & ACOSTA, A. J. 1976 Cavitation observations on axisymmetric bodies at supercritical Reynolds number. *J. Ship Res.* **20**, 40–50.

ARAKERI, V. H. & ACOSTA, A. J. 1981 Viscous effects in the inception of cavitation. *Trans. ASME* I: *J. Fluids Engng* **103**, 280–287.

ARNAL, D., HABIBALLAH, M. & COUSTOLS, E. 1984 Théorie de l'instabilité laminaire et critère de transition en écoulement bi et tri-dimensionnel. *La Recherche Aérospatiale* **2**.

AVELLAN, P., GINDROZ, B., HENRY, P., BACHMAN, P., VUILLOUD, A. & WEGNER, M. 1986 Influence de la chute d'essai et de la nucléation sur les performances en cavitation des modèles de turbines Francis. *AIRH Symp. on Cavitation and Turbomachinery, Montreal, August 1986.*

BRIANÇON-MARJOLLET, L. 1987 Couches limites, germes et cavités en interaction : étude physique. Thesis, University of Grenoble.

BRIANÇON-MARJOLLET, L. & MICHEL, J. M. 1987 The hydrodynamic tunnel of IMG : Former and recent equipment. *Proc. Intl. ASME Symp. on Cavitation Research Facilities and Techniques, Boston, Dec. 1987*, pp. 37–47.

FRANC, J. P. & MICHEL, J. M. 1985 Attached cavitation and the boundary layer : experimental investigation and numerical treatment. *J. Fluid Mech.* **154**, 63–90 (referred to herein as FM 1985).

FRANC, J. P. & MICHEL, J. M. 1988 Unsteady attached cavitation on an oscillating hydrofoil. *J. Fluid Mech.* **193**, 171–189 (referred to herein as FM 1988).

GATES, E. M. & ACOSTA, A. J. 1978 Some effects of several freestream factors on cavitation inception of axisymmetric bodies. *Proc. 12th Symp. on Naval Hydrodyn., Washington, DC, June 5–9*, pp. 86–110, National Academy Press.

HENRY, P., LECOFFRE, Y. & LARROZE, P. Y. 1980 Scale effects of cavitation phenomena. *AIRH Symp. on Cavitation and Fluid Machinery, Tokyo.*

HOLL, J. W. & CARROLL, J. A. 1979 Observations of the various types of limited cavitation on axisymmetric bodies. *Proc. Intl. ASME Symp. On Cavitation Inception, New York, Dec. 1979*, pp. 87–99.

HOLL, J. W. & WISLICENUS, G. F. 1961 Scale effects on cavitation. *Trans. ASME* D: *J. Basic Engng* 385–395.

HUANG, T. T. & PETERSON, F. B. 1976 Influence of viscous effects on model/full scale cavitation scaling. *J. Ship Res.* **20**, 215–223.

JOHNSON, V. E. & HSIEH, T. 1966 The influence of trajectories of gas nuclei on cavitation inception. *Proc. 6th Symp. on Naval Hydrodyn. Washington DC*, pp. 163–183.

KELLER, A. P. 1984 Scale effects at beginning cavitation applied to submerged bodies. *Proc. ASME Intl. Symp. on Cavitation Inception, New Orleans, Dec. 1984*, pp. 43–47.

KNAPP, R. T., DAILY, J. W. & HAMMIT, F. G. 1970 *Cavitation.* McGraw-Hill.

KODAMA, Y., TAMIYA, S., TAKE, N. & KATO, H. 1979 The effect of nuclei on the inception of bubble and sheet cavitation on axisymmetric bodies. *Proc. Intl. ASME Symp. on Cavitation Inception, New York, Dec. 1979*, pp. 75–80.

LECOFFRE, Y. 1987 Procedures and instrumentation for monitoring gas content in cavitation test loops. *Proc. Intl. ASME Symp. on Cavitation Research Facilities and Techniques, Boston, Dec. 1987*, pp. 139–146.

LECOFFRE, Y., BONNIN, J. 1979 Cavitation tests and nucleation control. *Proc. Intl. ASME Symp. On Cavitation Inception, New York, Dec. 1979*, pp. 141–145.

LE GOFF, J. P. & LECOFFRE, Y. 1982 Nuclei and cavitation. *Proc. 14th Symp. on Naval Hydrodyn., Ann Arbor*, pp. 215–242. National Academy Press.

LEMONNIER, H. & ROWE, A. 1988 Another approach in modelling cavitating flows. *J. Fluid Mech.* **195**, 557–580.

LINDGREN, H. & JOHNSSON, C. A. 1966 Cavitation inception on headforms. *Proc. 11th Intl. Towing Tank Conf., Tokyo.*

MENORET, L. & BLAYO, E. 1988 Effet du nombre de germes sur la cavitation à bulles et sur les pressions produites. *La Houille Blanche* **7/8**, pp. 501–505.

O'HERN, T. J., D'AGOSTINO, L. & ACOSTA, J. 1988 Comparison of holographic and Coulter counter measurements of cavitation nuclei in the ocean. *Trans. ASME* I: *J. Fluids Engng* **110**, 200–207.

OLDENZIEL, D. M. 1979 Bubble cavitation in relation to liquid quality. Thesis, Delft Hydraulics Laboratory publication N° 211.

PARKIN, B. R. & BAKER, B. B. 1988 Bubble dynamics and cavitation inception theory. *J. Ship Res.* **23**, 155–167.

PELLONE, C. & ROWE, A. 1981 Supercavitating hydrofoils in non-linear theory. *Proc. 3rd Intl. Conf. on Numerical Ship Hydrodyn., Paris*, pp. 399–412.

PLESSET, M. S. & PROSPERETTI, A. 1977 Bubble dynamics and cavitation. *Ann. Rev. Fluid Mech.* **9**, 145–185.

VAN DER MEULEN, J. H. J. 1980 Boundary layer and cavitation studies of NACA 16-012 and NACA 4412 hydrofoils. *Proc. 13th Symp. on Naval Hydrodyn., Tokyo*, pp. 195–219, National Academy Press.

VOINOV, O. V. 1973 On the force acting on a sphere in a non-uniform stream of perfect incompressible fluid. *J. Appl. Mech. Tech. Phys.* **4**, pp. 182–184.